GRAS SAF Visiting Scientist activity No. 15
CM SAF Visiting Scientist activity No. 2.11

Climate Monitoring using GRAS data within the CM-SAF Humidity Composite Product

Joint Visiting Scientist Study
of
CM-SAF and GRAS-SAF

by
Ralf Lindau

Version 3.0
20.02.2008

Contents

Preface **iii**

1 Introduction **1**

2 Data **1**
2.1 ATOVS data and procedures 2
2.2 CHAMP Data 4
2.3 Radiosonde Data 5

3 Comparison of ATOVS with radiosondes **5**

4 Comparison of ATOVS to CHAMP data **11**
4.1 Data preparation and observation matching 11
4.2 Difference statistics for match-ups 14
4.3 Global maps of differences 15

5 Conclusions **18**

List of Figures

1 *Example for the krigged daily global fields from ATOVS. The figure shows the Layered Precipitable Water between 300 and 500 hPa for 1 October 2004 on a spatial resolution of 90 km.* . . . 2
2 *As Fig.1, but for the error.* . . . 2
3 *Monthly mean of Total Precipitable Water as retrieved by ATOVS for October 2004.* . . . 3
4 *Standard deviation of 31 daily means of Total Precipitable Water at each location for October 2004 as retrieved by ATOVS.* . . . 3
5 *Available observation from CHAMP during one month. Total Precipitable Water for October 2004 is shown as coloured spots for each instantaneous point measurement.* . . . 4
6 *Locations of 173 GUAN radiosonde stations used as ground truth.* . . . 4
7 *Daily mean Total Precipitable Water as retrieved from ATOVS compared to radiosonde measurements.* . . . 5
8 *Variance of vapour included within different time and space scales derived from GPS stations in Scandinavia (Lindau, 2000). Crosses depict equal variance in space and time in steps of 1 kgm^{-2}. Read example: In a square of 980 km by 980 km the same amount of variance is instantaneously existent as at a fixed location during 95 hours. The amount of variance is for this case 19 mm^2.* . . . 5
9 *As Fig.7, but for the layer 1000 - 850 hPa.* . . . 6
10 *As Fig.7, but for the layer 700 - 500 hPa.* . . . 6
11 *Temporal evolution of the bias of ATOVS-derived water vapour content using radiosonde measurements as reference. The line indicated by 0 shows the vertically integrated water vapour, the 5-line denotes the layer between 1000 hPa and 0 hPa, the 4-line is the layer between 850 hPa and 700 hPa.* . . . 10
12 *Temporal evolution of the RMS (R) of TPW between ATOVS-derived TPW and radiosonde measurements from GUAN stations. The RMS is decomposed into the bias (B) and the bias corrected RMS (C). The B-line of this figure is equal to the 0-line of Fig 11.* . . . 10
13 *Monthly means for October 2004 of TPW from ATOVS compared to the according radiosonde means at each GUAN station. Monthly means are calculated only if at least 15 daily means are available.* . . . 11
14 *As Fig.13, but with weighted statistics, so that the overall data statistics as mean and standard deviation do not differ from those derived from daily means (Fig.7).* . . . 11
15 *Spatial and temporal distances of observation pairs from CHAMP and ATOVS in October 2004, given in logarithmic scales. Vertical and horizontal lines denote the average distances of about 3 hours and 70 km, respectively.* . . . 13
16 *Comparison of TPW from ATOVS with CHAMP observations. The data is based on match-ups using next neighbouring ATOVS observation from NOAA-15.* . . . 13
17 *As Fig.16, but for LPW 3 (700 - 500 hPa).* . . . 14
18 *As Fig.16, but for LPW 4 (850 - 700 hPa).* . . . 14
19 *Difference of Total Precipitable Water between CHAMP and ATOVS in October 2004.* . . . 17
20 *As Fig.19, but for Layer 5 (1000 hPa - 850 hPa).* . . . 17
21 *As Fig.19, but for Layer 4 (850 hPa - 700 hPa).* . . . 17
22 *As Fig.19, but for Layer 3 (700 hPa - 500 hPa).* . . . 17
23 *As Fig.19, but for Layer 2 (500 hPa - 300 hPa).* . . . 17
24 *As Fig.19, but for Layer 1 (300 hPa - 200 hPa).* . . . 17

Preface

This text contains the results of the first joint Visiting Scientist study of GRAS- and CM-SAF. As the work proceeded during the redevelopment of the ATOVS temperature and water vapour product at CM-SAF several recurrences of the comparisons have been performed. A major issue was a ATOVS processing error at CM-SAF that led to large biases of derived water vapour contents compared to radiosondes. Upon completion of this text another defect in the quality control of the radiosonde data was detected at CM-SAF (incomplete radiosonde profiles with missing lower atmosphere were included in the comparison). By now CM-SAF performed a complete validation of ATOVS-derived water vapour contents with radiosondes over the period 2004-2007. Systematic errors throughout the period are much smaller than described in this report (Figures 7-12 and Table 2a) whereas random errors are comparable. Thus, conclusions with respect to radiosonde data have to be interpreted with care. However, the systematic differences as well as the spatial distribution of these differences to CHAMP are real and not affected.

Both SAFs perceived this study as a very useful start of further collaborations in this field and look forward to improved analysis of differences between water vapour estimates from the MetOp instruments.

Jörg Schulz, Deutscher Wetterdienst
Offenbach, 27 March 2008

1 Introduction

Humidity products can be derived from a large range of different satellite sensors including infrared and microwave sounders and imagers, VIS spectrometer and radio occultation instruments. Within the Satellite Application Facility (SAF) on Climate Monitoring (CM-SAF), data from the SEVIRI (Spinning Enhanced Visible and Infrared Imager) instrument on the geostationary Meteosat satellite, the ATOVS (Advanced TIROS Operational Vertical Sounder) infrared and microwave instrument suite onboard the polar-orbiting NOAA (National Oceanic and Atmospheric Administration) and METOP (Meteorological Operational) platforms, the IASI (Infrared Atmospheric Sounding Interferometer) instrument on METOP and the microwave radiometer SSM/I (Special Sensor Microwave Imager) onboard DMSP (Defense Meteorological Satellite Program) platforms are used to develop a water vapor climatology. From its system version 3 onwards, CM-SAF will provide global estimates for individual instrument records.

The SAF on GRAS (Global navigation satellite Receiver for Atmospheric Sounding) Meteorology (GRAS-SAF) is dedicated to radio occultation measurements from the EPS (EUMETSAT Polar System) METOP satellite, focusing on the Global Positioning System (GPS) instrument of GRAS. GRAS data is expected to improve on the traditional sounder products in the upper troposphere and lower stratosphere as well as under rainy conditions. Although the spatiotemporal sampling of the GRAS instrument is not as good as of other imagers or sounders, GRAS data can be used to construct an alternative single source climate product.

The main objective of the joint visiting scientist activity of the GRAS-SAF and the CM-SAF is the investigation of the potential role of GRAS data within the humidity product suite of CM-SAF. Within this study, a comprehensive intercomparison of CHAMP (CHAllenging Minisatellite Payload), ATOVS, and ground based temperature and mixing ratio profiles in order to understand systematic differences between radio occultation and atmospheric sounder estimates better will be performed. The understanding of the systematic differences between water vapor estimates based on totally different measurement principles is considered to be a prerequisite for the application of merging algorithms to data from different instruments into a so-called best climate data set. ATOVS and CHAMP data are used to construct daily, monthly, and seasonal maps of integrated water vapor that are analyzed with respect to the different representation of spatial and temporal variability in the data sets. From this analysis it might be deducted on what spatiotemporal scales the individual estimates are best usable for the purpose of climate monitoring.

2 Data

In this study two satellite products for atmospheric humidity are analysed. The first is derived from Advanced TIROS Operational Vertical Sounder (ATOVS) instrument data; the second is based on atmospheric soundings of CHAMP. Both products are cross-checked by radiosonde measurements. A comprehensive mutual comparison of all three data sets is hampered by the fact that only NOAA satellites provide global area-covering information, whereas the other two consists of point measurements at a few stations (radiosondes) or sporadically distributed over the globe (CHAMP).

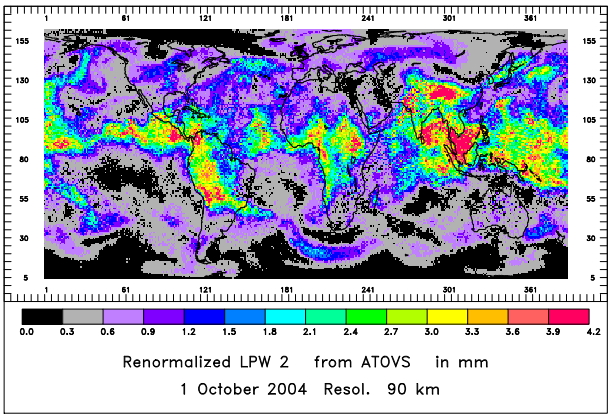

Figure 1: *Example for the krigged daily global fields from ATOVS. The figure shows the Layered Precipitable Water between 300 and 500 hPa for 1 October 2004 on a spatial resolution of 90 km.*

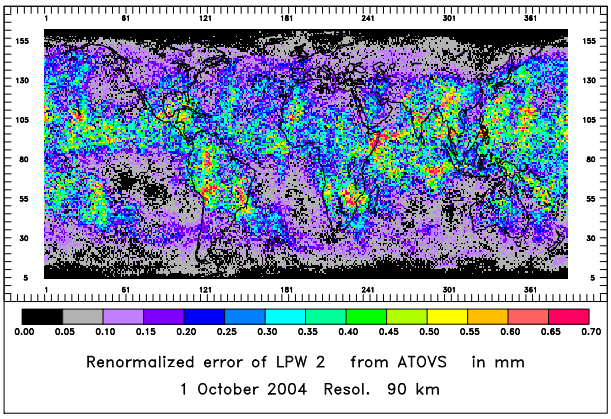

Figure 2: *As Fig.1, but for the error.*

2.1 ATOVS data and procedures

The first investigated humidity product uses infrared and microwave observations from ATOVS onboard the polar-orbiting NOAA-15 and NOAA-16 platforms. The retrieval is based on the International ATOVS Processing package (IAPP) (Li et al., 2000) using measurements from AMSU (Advanced Microwave Sounding Unit) and HIRS (High Resolution Infrared Radiation Sounder) to retrieve the atmospheric temperature and humidity profiles as well as some cloud properties. As additional information weather forecasts of the atmospheric temperature, humidity and surface pressure provided by the DWD (Deutscher Wetterdienst) model GME (Global Model Europe) are used within the retrieval as first guess. In the raw data delivered by the Satellite Application Facility on Climate Monitoring (CM-SAF) vertical profiles of humidity and temperature are given as vertically integrated water vapor content and mean layer temperature in 5 layers (Tab.1).

The data is further processed by a Kriging technique to optimally merge data from the two NOAA platforms and to produce fully covered daily fields for all layers together with an error map. The technique does not prescribe a fixed radius in which observations are considered at all, as performed in ordinary block Kriging. (Lindau et al., 2004; Lindau, 2005).The technique manages the aggregation of additional information step by step, deciding at each stage which observation could contribute a maximum of new, not redundant information. This depends on three characteristics of the potentially added observation: its distance to the predicting point, its individual error and its redundancy with the already aggregated observations.

Tab.1 Boundaries of vertical layers.

Vertical Layer	Pressure boundaries / hPa
1	200 - 300
2	300 - 500
3	500 - 700
4	700 - 850
5	850 - 1000

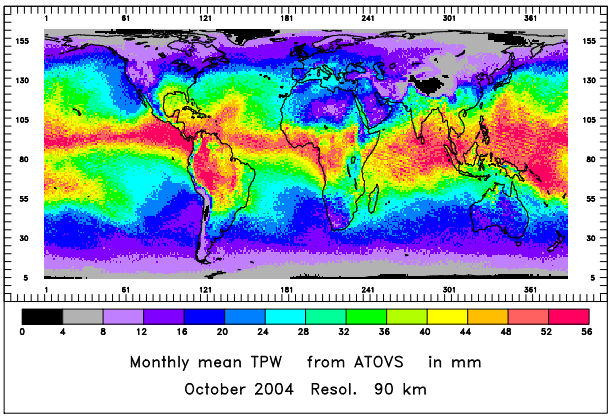

Figure 3: *Monthly mean of Total Precipitable Water as retrieved by ATOVS for October 2004.*

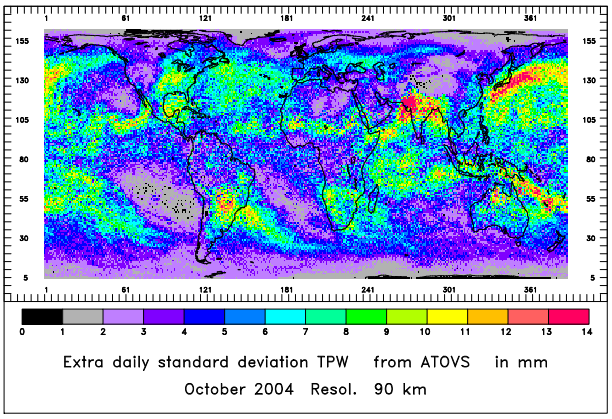

Figure 4: *Standard deviation of 31 daily means of Total Precipitable Water at each location for October 2004 as retrieved by ATOVS.*

Two pieces of information are necessary to run the Kriging procedure. These are (i) the spatial correlation function and (ii) the error of each observation. (i) The correlation function is derived to have an estimate how fast the information content of an observation is decreasing with increasing distance. It is derived by fitting a quadratic exponential function to the data. Errors are definitely affecting the correlation function. However, it can be shown (Lindau, 2003) that their impact can be easily corrected by a constant factor. (ii) The error variance of each individual observation is derived by decomposing the total variance at each grid point into an external and an internal part. In the case of daily averages the external ind internal parts would be extra- and intra-daily variability. For this purpose, the data is binned into daily 90 km grid boxes. The mutual variance of such averages is considered as external, the remaining variance within each of these boxes is regarded as internal. From the internal variance, the errors are concluded. However, in this aspect the number of independent observations is crucial. Concerning satellite data, independence of pixels is a daring assumption. In fact, the analysis of variance revealed that only grid point averages of different satellites or instruments can be regarded as independent (Lindau and Schulz, 2004).

Thus, ATOVS data is available in three stages of processing. (i) Scan-oriented individual pixels separately for NOAA-15 and NOAA-16. (ii) Daily averages of both platforms on a 90-km grid. (iii) Fully covered krigged field on the same spatial and temporal resolution. For each of these daily fields an error field is computed. Figs. 1 and 2 give an example for the 1 October 2004 and the layer between 500 and 300 hPa. The monthly mean is then concluded by averaging the daily means. Figure 3 shows the monthly mean of Total Precipitable Water (TPW) for October 2004. A tropical band of high moisture is apparent connected with the warm air masses in low latitudes. Over high mountain regions as Himalayas and Andes the remaining upper part of the troposphere contains as expected only extreme few water vapour. Therefore, sharp gradients of moisture occur for example at the western slope of Ethiopian Highlands which will be discussed in detail in section 4.3. The temporal variance of TPW (Fig.4) gives an idea of the accuracy of monthly means. Most regions show standard deviations of less than 5 to 6 mm which means that the accuracy of monthly means is below 1 mm (Division by square root of 31). Only in some regions as e.g. over India or Japan the variability is increased due to Monsoon and Kuro Shio, respectively.

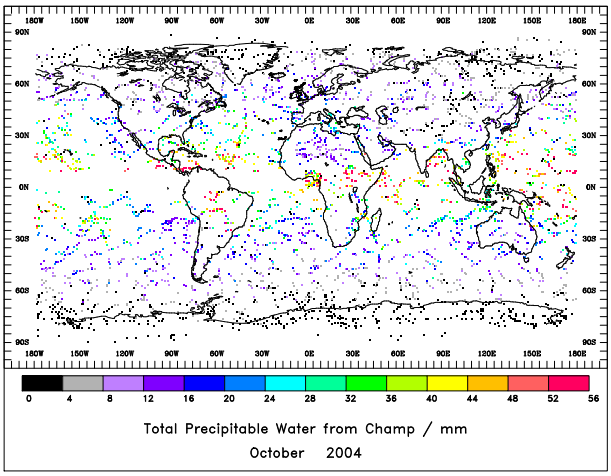

Figure 5: *Available observation from CHAMP during one month. Total Precipitable Water for October 2004 is shown as coloured spots for each instantaneous point measurement.*

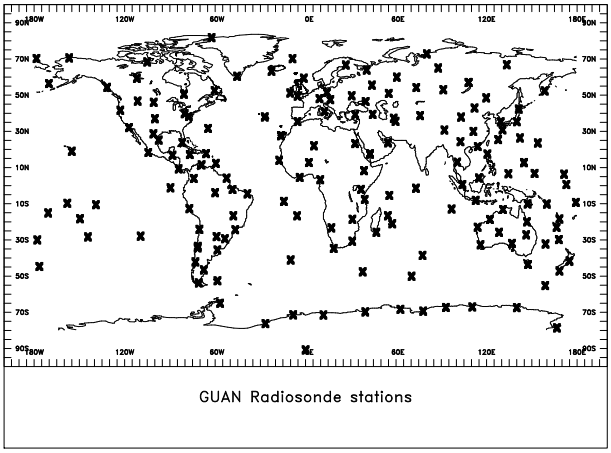

Figure 6: *Locations of 173 GUAN radiosonde stations used as ground truth.*

2.2 CHAMP Data

A rather new method for the indirect measurement of temperature, pressure and water vapor in the stratosphere and the troposphere is based on atmospheric limb sounding by using the continuously broadcasted radio signals from the Global Navigation Satellite System (GNSS) satellites. The electron density in the ionosphere, the temperature, pressure and water vapor in the atmosphere influence these signals. The GNSS signals are delayed on the way through the ionosphere and atmosphere during the radio occultation. As a result, the ray path is slightly bent. This is observed in the amplitude and phase of the received signal on a Low-Earth Orbit (LEO) satellite seeing a GNSS satellite. Using inversion methods and geometrical considerations, the computation of a profile of the atmospheric refractivity at the position where the individual ray path has passed closest to the surface is possible if the position and velocity of the LEO and GNSS satellite are known. The refractivity is calculated using the Abel transform inversion method. The so-called dry temperature and pressure are obtained using the ideal gas law assuming hydrostatic equilibrium. Using ancillary data from an NWP model as temperature and humidity profiles as well as surface pressure being appropriate in time and location of the occultation, the temperature and humidity profiles are calculated in combination with the refractivity in a 1DVAR algorithm. A more detailed description of the principles can be found in, e.g., Wickert et al. (2004). As the radio occultation measurements are absolute, no calibration is needed. The observation geometry for one satellite leads to a global coverage of the products. One advantage of the radio occultation method is the high vertical resolution of the products and its insensitivity to clouds and rain.

Beside its original navigation purpose, GPS satellites are used in meteorological science since many years to determine the atmospheric humidity. So far, ground based receivers determine the humidity from the signal delay caused by water vapour. The innovative approach of CHAMP is that a GPS receiver is launched to orbit. Whenever, the signal from a GPS satellite passes on its way to CHAMP through the atmosphere, the vertical water vapour distribution can be derived by the so-called Radio Occultation technique. This causes an irregular and relatively sparse distribution of CHAMP observations. For satellite data the total observation number is relatively small with about 4000 observations per month, sporadically spreaded over the globe (Fig.5).

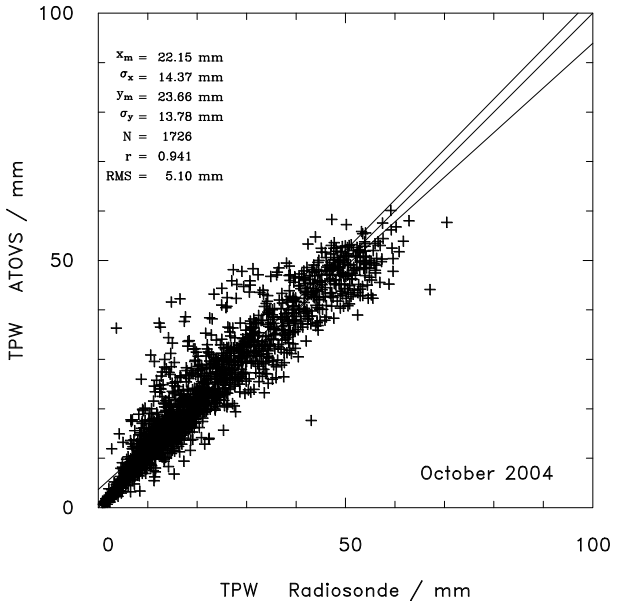

Figure 7: *Daily mean Total Precipitable Water as retrieved from ATOVS compared to radiosonde measurements.*

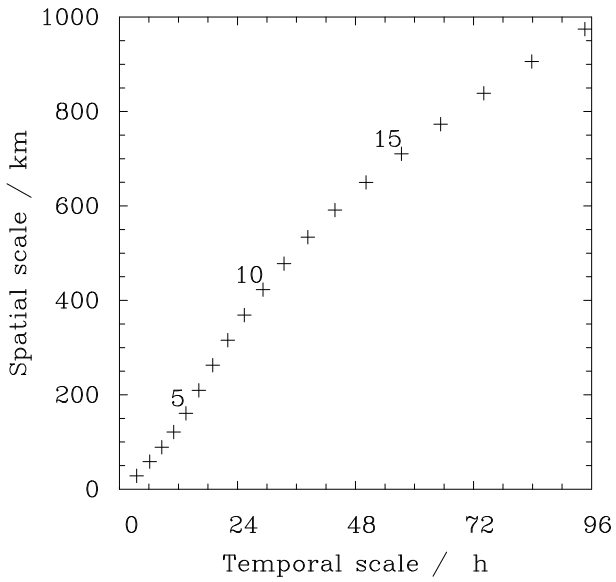

Figure 8: *Variance of vapour included within different time and space scales derived from GPS stations in Scandinavia (Lindau, 2000). Crosses depict equal variance in space and time in steps of 1 kgm^{-2}. Read example: In a square of 980 km by 980 km the same amount of variance is instantaneously existent as at a fixed location during 95 hours. The amount of variance is for this case 19 mm^2.*

2.3 Radiosonde Data

In order to assess the quality of satellite observations independent ground based measurements are used. GCOS (Global Climate Observing System) has designated a subset of their radiosonde network: The GCOS Upper-Air Network (GUAN). GUAN consists of 173 radiosonde stations fairly evenly distributed over the globe (Fig.6), so that an unbiased global comparison is possible. As for ATOVS data, GUAN data is preprocessed by DWD. The vertically high resolved measurements of temperature and humidity are averaged over 5 layers corresponding to the ATOVS data (Tab.1).

3 Comparison of ATOVS with radiosondes

Fig.7 shows a comparison of the total column precipitable water (TPW) as retrieved from ATOVS with radiosonde measurements from the 173 worldwide distributed GUAN stations during October 2004. A wet bias of approximately 1.5 mm for the ATOVS data is obvious. Before investigating this problem in detail, we first consider the comparability of temporal and spatial scales of the two involved data sets.

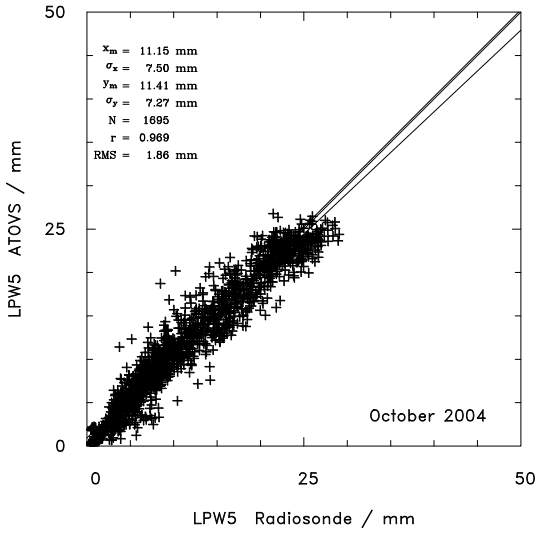

Figure 9: *As Fig.7, but for the layer 1000 - 850 hPa.*

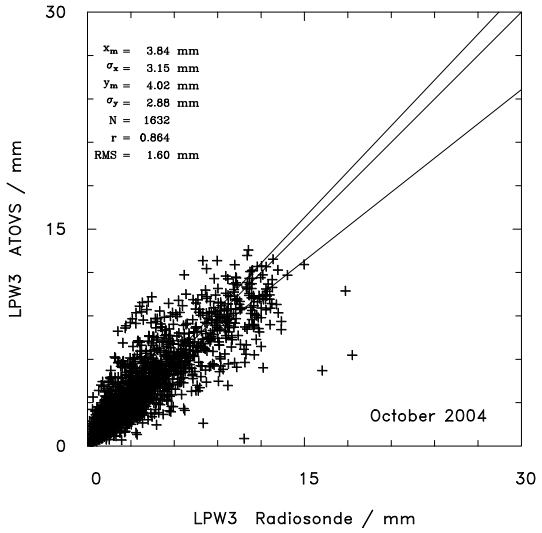

Figure 10: *As Fig.7, but for the layer 700 - 500 hPa.*

After the applied kriging routine ATOVS data represent averages over 90 by 90 km^2 in space and 24 hours in time, whereas radiosondes can be regarded as point measurements. To compensate for the different temporal resolution, the radiosonde data is averaged over one day, so that only days with at least 2 ascents could be taken into account. However, the spatial resolution of both data sets is still different. The mean spatial variance of daily means within a box of 90 by 90 km^2 is averaged out in the ATOVS data.

Lindau and Ruprecht (2000) estimated the variance of TPW on different temporal and spatial scales from GPS (Global Positioning System) measurements (Fig.8). They found a mean temporal variance within one day of about 8 mm^2. Spatially, the variance was about 3 mm^2 for the 90-km scale. As their study is based on individual measurements, an amount of 3 mm^2 is the upper limit for the variability of daily means (with 90 km resolution), because the variance of daily means should be lower than the variance of high resolution data. The magnitude of the missing spatial variance (0 - 3 mm^2) within ATOVS data is small compared to the total variance considered in Fig.7 (190 mm^2, corresponding to a standard deviation of 13.78 mm), so that this effect can be neglected.

For daily means the correlation coefficient of the Total Precipitable Water from ATOVS and from radiosondes is 0.941 (Fig.7). Correlations less than 1 are generally obtained due to random errors in the compared observations. For one data set, the krigged TPW fields from ATOVS, the daily error fields are available as they are an inherent result of the kriging technique itself. Fig. 2 shows an example for the 1 October 2004. For those 173 grid boxes where radiosonde data is available the monthly mean error variance is $\epsilon^2_{AT} = 5.57\, mm^2$.

For the other data set, the radiosonde measurements, an estimate for the observation error of daily means is obtained by dividing the internal daily variance by the observation number. The resulting mean error variance is $\epsilon^2_{RS} = 7.65\, mm^2$. Thus, the uncertainties of both data sets are comparable with about 6.5 mm^2.

How much of the scatter visible in Fig.7 arises directly from such unavoidable observation errors in both

data sets? Is the correlation coefficient of 0.941 expectable with regard to the errors? These questions are discussed in the following. The correlation coefficient is defined as:

$$r = \frac{\sigma_{xy}}{\sigma_x \sigma_y} \tag{1}$$

where σ_x and σ_y denote the variance of the two compared data sets and σ_{xy} their covariance. Errors cause a spurious increase of the both variances, but leave the covariance unchanged if the errors are random. Consequently, errors ϵ_x and ϵ_y reduce the correlation coefficient to:

$$r_{err} = \frac{\sigma_{xy}}{\sqrt{(\sigma_x^2 + \epsilon_x^2)(\sigma_y^2 + \epsilon_y^2)}} \tag{2}$$

If both true variances and observation errors are assumed to be equal for both data sets i.e. $\sigma_x = \sigma_y = \sigma$ and $\epsilon_x = \epsilon_y = \epsilon$, the effect of errors can be estimated by:

$$\frac{r_{err}}{r} = \frac{\sigma^2}{\sigma^2 + \epsilon^2} \tag{3}$$

Assuming a perfect true correlation apart from error effects (r=1), the correlation reduction due to errors is equal to:

$$1 - r_{err} = \frac{\epsilon^2}{\sigma^2 + \epsilon^2} \tag{4}$$

where σ^2 and ϵ^2 denote natural and error variance. The sum of natural and error variance can be taken from Fig.7. For both data sets the total variance is comparable with about $200mm^2$, as both ATOVS and radiosondes show standard deviations of approximately 14 mm. Following Eq.(4) the expected correlation reduction is:

$$1 - r_{err} = \frac{6.5mm^2}{200mm^2} = 0.033 \tag{5}$$

Thus, more than half of the scatter in Fig.7 (Reduction of correlation coefficient by 0.059) can be explained by the random errors in both data sets.

However, Fig.7 shows a wet bias of ATOVS water vapour of about 7%, which shall be discussed in the following. To get an idea of the reason for this bias we expanded the comparison over two years from January 2004 to December 2005 and distinguished additionally between different vertical layers. Figs. 9 and 10 show two examples for the precipitable water in the lowest layer (between 1000 hPa and 850 hPa) and the mid-tropospheric layer (between 700 hPa and 500 hPa). The bias persists in both levels, but is reduced, also if considered as relative deviation. Tab.2 summarizes the results for all layers and month. Strongest overestimation appears in the second lowest atmospheric layer (Layer 4, 850 to 700 hPa) with biases of more than 10%. In the neighbouring levels, at ground and in the mid atmosphere, wet biases of a few percent prevail. Between 500 and 300 hPa (layer 2) the bias vanishes or is even negative in most months. The highest layer contains only a very small percentage of the total atmospheric water vapour (approx. 1%) so that the relative accuracy of observation is low. Correlation coefficients are reduced to about 0.5 compared to values of 0.8 in layer 2 and more than 0.95 at the surface. Having in mind both the low accuracy and the low absolute humidity in the top layer, we should not overinterpret that the dry

biases of ATOVS exceed 20%. However, it is a common feature of all considered months.

Tab.2a Comparison of Layered and Total Precipitable Water as retrieved by ATOVS and measured by GUAN radiosondes. For all in months in 2004 and five layers the correlation r and the bias (ATOVS - RS) in mm and in percent are given.

Month	Layer	0	1	2	3	4	5
04/01	Bias mm	1.41	-0.03	-0.03	0.11	0.56	0.33
	Bias %	7	-28	-3	3	9	3
	r	0.959	0.640	0.862	0.905	0.945	0.976
04/02	Bias mm	1.90	-0.02	-0.01	0.23	0.76	0.41
	Bias %	9	-23	-1	6	13	4
	r	0.950	0.632	0.890	0.911	0.931	0.968
04/03	Bias mm	1.19	-0.02	0.01	0.08	0.47	0.21
	Bias %	6	-20	1	2	8	2
	r	0.960	0.624	0.890	0.911	0.945	0.976
04/04	Bias mm	1.46	-0.03	0.03	0.21	0.55	0.28
	Bias %	7	-26	2	5	9	3
	r	0.958	0.554	0.860	0.902	0.938	0.972
04/05	Bias mm	1.59	-0.02	0.01	0.28	0.72	0.26
	Bias %	7	-21	1	6	10	2
	r	0.956	0.638	0.880	0.910	0.931	0.968
04/06	Bias mm	1.61	-0.06	-0.01	0.23	0.78	0.36
	Bias %	6	-45	-1	5	10	3
	r	0.949	0.128	0.870	0.904	0.916	0.960
04/07	Bias mm	1.52	-0.04	-0.03	0.14	0.86	0.31
	Bias %	5	-30	-2	3	10	2
	r	0.951	0.545	0.880	0.909	0.913	0.949
04/08	Bias mm	1.31	-0.04	0.00	0.13	0.77	0.23
	Bias %	5	-28	0	2	9	2
	r	0.955	0.676	0.874	0.910	0.924	0.953
04/09	Bias mm	1.25	-0.03	-0.02	0.12	0.77	0.20
	Bias %	5	-29	-2	3	10	2
	r	0.951	0.659	0.844	0.894	0.914	0.954
04/10	Bias mm	1.51	-0.02	0.00	0.18	0.75	0.26
	Bias %	7	-25	0	5	11	2
	r	0.941	0.576	0.774	0.864	0.910	0.969
04/11	Bias mm	1.14	-0.02	-0.03	0.10	0.63	0.08
	Bias %	6	-24	-3	3	11	1
	r	0.949	0.537	0.795	0.875	0.932	0.972
04/12	Bias mm	1.66	-0.02	0.01	0.11	0.76	0.36
	Bias %	9	-26	1	3	14	4
	r	0.947	0.593	0.851	0.897	0.931	0.970

Tab.2b As Table 2a, but for the year 2005.

Month	Layer	0	1	2	3	4	5
05/01	Bias mm	1.78	-0.03	-0.02	0.17	0.77	0.31
	Bias %	9	-28	-2	5	14	3
	r	0.952	0.648	0.877	0.904	0.939	0.975
05/02	Bias mm	1.86	-0.03	-0.01	0.22	0.76	0.32
	Bias %	9	-29	0	6	13	3
	r	0.944	0.469	0.855	0.890	0.930	0.974
05/03	Bias mm	1.18	-0.03	-0.01	0.08	0.62	0.15
	Bias %	6	-32	-1	2	10	2
	r	0.949	0.428	0.835	0.898	0.927	0.975
05/04	Bias mm	1.15	-0.04	-0.03	0.12	0.48	0.09
	Bias %	6	-34	-3	3	8	1
	r	0.940	0.532	0.827	0.882	0.929	0.963
05/05	Bias mm	1.09	-0.03	-0.07	0.10	0.65	-0.03
	Bias %	5	-27	-6	2	9	0
	r	0.937	0.564	0.801	0.879	0.901	0.961
05/06	Bias mm	1.63	-0.03	-0.03	0.20	0.85	0.32
	Bias %	6	-24	-2	4	10	2
	r	0.949	0.642	0.864	0.897	0.916	0.963
05/07	Bias mm	1.83	-0.02	-0.04	0.20	0.94	0.48
	Bias %	6	-17	-3	4	11	3
	r	0.952	0.679	0.887	0.904	0.928	0.944
05/08	Bias mm	1.30	-0.03	-0.06	0.07	0.79	0.22
	Bias %	4	-20	-4	1	9	2
	r	0.954	0.630	0.868	0.910	0.929	0.957
05/09	Bias mm	1.28	-0.03	-0.02	0.08	0.76	0.16
	Bias %	5	-26	-2	2	10	1
	r	0.949	0.601	0.854	0.891	0.921	0.968
05/10	Bias mm	1.33	-0.02	0.00	0.13	0.69	0.19
	Bias %	6	-23	0	3	10	2
	r	0.950	0.582	0.788	0.885	0.928	0.970
05/11	Bias mm	1.67	-0.02	-0.06	0.16	0.67	0.34
	Bias %	8	-23	-5	4	11	3
	r	0.951	0.721	0.856	0.917	0.941	0.972
05/12	Bias mm	1.31	-0.03	-0.08	0.05	0.54	0.24
	Bias %	7	-28	-7	1	10	3
	r	0.965	0.642	0.888	0.928	0.958	0.978

In Fig.11 the temporal evolution of the wet bias during a two years period is shown for three cases: The vertically integrated water vapour and for the two lowest layers up to 850 hPa, and 700 hPa, respectively. Biases for the three highest layers are too small to be depicted in Fig.11, but can be taken from Table 2. We can conclude that the bias seems to be constant throughout the year and that it is strongest in the second lowest atmospheric layer.

Some communities prefer to express deviations between two data sets in terms of root mean square (rms) difference:

$$rms = \sqrt{\overline{\sum_{i=1}^{n} (x_i - y_i)^2}} \tag{6}$$

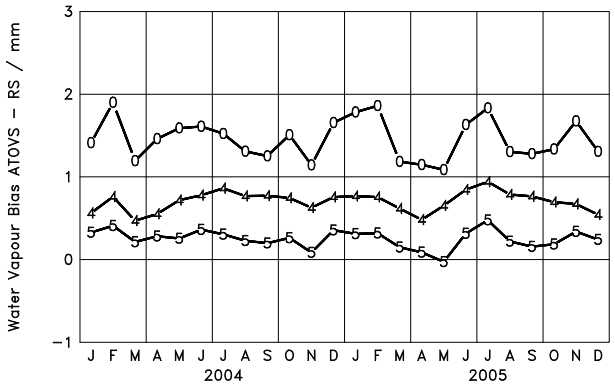

Figure 11: *Temporal evolution of the bias of ATOVS-derived water vapour content using radiosonde measurements as reference. The line indicated by 0 shows the vertically integrated water vapour, the 5-line denotes the layer between 1000 hPa and 0 hPa, the 4-line is the layer between 850 hPa and 700 hPa.*

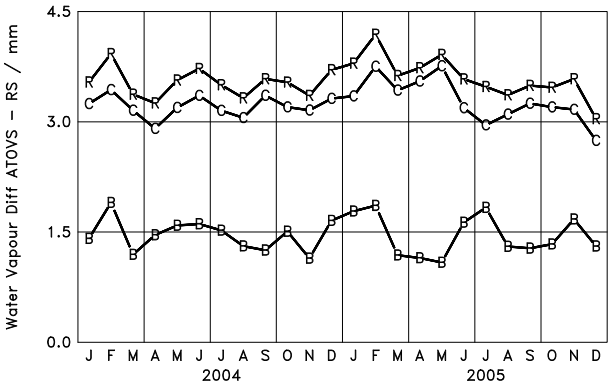

Figure 12: *Temporal evolution of the RMS (R) of TPW between ATOVS-derived TPW and radiosonde measurements from GUAN stations. The RMS is decomposed into the bias (B) and the bias corrected RMS (C). The B-line of this figure is equal to the 0-line of Fig 11.*

instead of bias and correlation as we did so far. However, then it is appropriate to distinguish between the two components of the rms, the bias corrected rms (bcr) and the bias itself, which are connected by:

$$rms^2 = bcr^2 + bias^2 \tag{7}$$

The evolution of these three terms for the differences in Total Precipitable Water from ATOVS and radiosondes during the period January 2004 to December 2005 is given in Fig.12. The RMS is dominated by pure scatter (bcr), the contribution of biases is limited. Both components seem to remain essentially constant during time.

So far we considered daily means in our comparisons. The next issue investigated is concerned with the behaviour of monthly means. For each of the radiosonde stations the daily means are averaged over one month and compared to the corresponding means of ATOVS. Fig.13 shows the result for TWP for October 2004. The RMS is reduced to 3.72 mm compared to 5.10 mm found on the base of daily means (Fig.7). The reduction reflects the diminished random errors of monthly means caused by 30 times more observations available. The reverse effect of increased internal variance from daily to monthly scale is by far overcompensated. In Fig.13 only months with at least 15 days of observation are taken into account. Unfortunately, this proceeding has the consequence that daily and monthly statistics are not comparable because the data base is slightly changed. The overall means differ arbitrary and the reduction of standard deviation can not be strictly assigned to the removal of variance which is expected when monthly instead of daily means are considered. Unwanted shifts in statistic are avoided by weighted characteristics (Fig.14). Here the overall means are conserved and changes in the other statistics are correctly interpretable. The results for other months are summarized in Table 3.

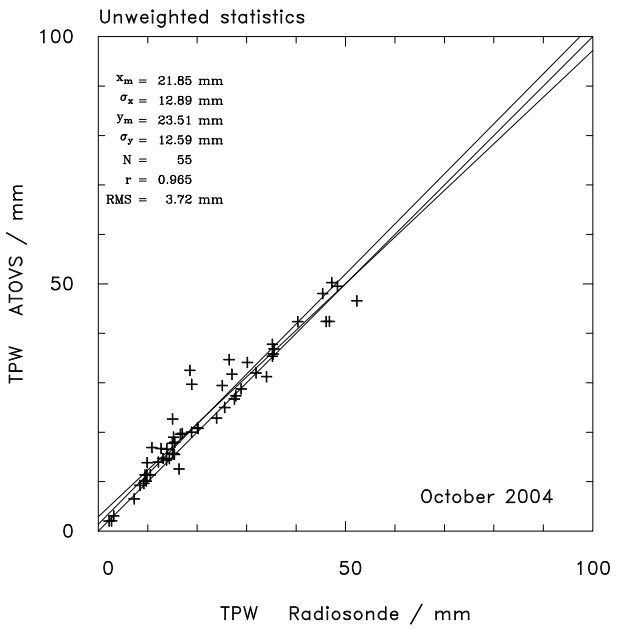

Figure 13: *Monthly means for October 2004 of TPW from ATOVS compared to the according radiosonde means at each GUAN station. Monthly means are calculated only if at least 15 daily means are available.*

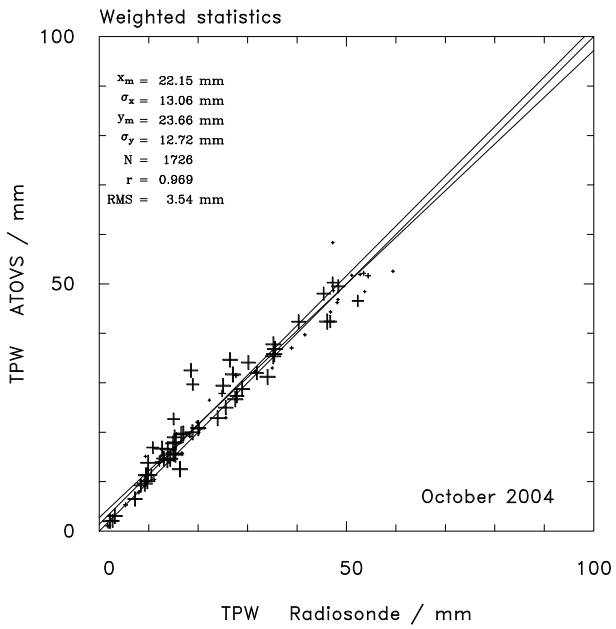

Figure 14: *As Fig.13, but with weighted statistics, so that the overall data statistics as mean and standard deviation do not differ from those derived from daily means (Fig.7).*

4 Comparison of ATOVS to CHAMP data

4.1 Data preparation and observation matching

CHAMP data as provided by DMI comprise three parameters, geopotential height, temperature and specific humidity on 43 fixed pressure levels from 1013.3 hPa up to 0.1 hPa. About each 10 minutes one individual observation is available somewhere on the globe, so that per month about 4000 irregularly distributed observations are available. This makes a direct comparison to radiosondes difficult because coincident measurements from both observing systems are very rare. However, except for the poles ATOVS data has a complete global coverage and can serve as link between the point informations from CHAMP and radiosondes.

To make the vertical resolution comparable to ATOVS, we integrated Champ RO data over the five layers in which ATOVS data is available (Table 1). The vertical integration of specific humidity q in pressure coordinates according to:

$$LPW = \frac{1}{g} \int_{p_1}^{p_2} q dp \tag{8}$$

yields the water vapour content LPW between the pressure levels p_1 and p_2. The acceleration of gravity g is assumed to be constant with 9.8 ms^{-2}. Using Eq.(8), the TPW and five LPWs for the layers between 1000 and 200 hPa are calculated. Additionally, the amounts of water vapour lying below 1000 and above 200 hPa are stored. Since the pressure levels in CHAMP data (e.g. 702.7 followed by 656.4 hPa) differ

Table 3: Monthly mean Total Precipitable Water as provided by GUAN radiosondes (R) and as retrieved by ATOVS (A). The overall means and standard deviations between the stations are given as well as correlation coefficient r and the number of observations N. As weighted statistics are applied N is equal to the overall sum of daily means and do not reflect the number of stations involved. Further columns give the bias induced variance (bias var) and its complementary variance contribution of pure scatter by the bias corrected RMS. Their sum gives the squared RMS (rms var).

Year	Month	R mean	R stddev	A mean	A stddev	N	r	bias var	bcr var	rms var	rms
2004	1	20.07	15.81	21.49	16.09	1518	0.9794	1.99	10.53	12.52	3.54
2004	2	20.45	15.73	22.35	16.26	1487	0.9775	3.61	11.80	15.41	3.93
2004	3	20.68	15.88	21.88	15.83	1503	0.9802	1.43	9.95	11.38	3.37
2004	4	21.93	14.76	23.39	14.98	1518	0.9810	2.13	8.45	10.59	3.25
2004	5	23.97	15.04	25.56	14.83	1590	0.9772	2.53	10.19	12.72	3.57
2004	6	25.29	14.10	26.90	13.96	1485	0.9714	2.59	11.27	13.86	3.72
2004	7	27.92	14.30	29.45	14.18	1576	0.9755	2.32	9.94	12.26	3.50
2004	8	28.06	14.38	29.37	14.45	1627	0.9775	1.71	9.33	11.04	3.32
2004	9	25.89	14.58	27.15	14.51	1541	0.9734	1.57	11.27	12.84	3.58
2004	10	22.15	13.06	23.66	12.72	1726	0.9695	2.27	10.24	12.52	3.54
2004	11	20.44	13.31	21.58	13.63	1581	0.9728	1.31	9.96	11.27	3.36
2004	12	19.33	13.50	20.98	13.75	1558	0.9706	2.74	10.99	13.73	3.71
2005	1	19.12	14.96	20.90	15.37	1481	0.9759	3.18	11.22	14.40	3.79
2005	2	20.38	15.02	22.24	15.63	1287	0.9708	3.46	14.08	17.54	4.19
2005	3	20.42	14.82	21.61	15.02	1538	0.9737	1.40	11.75	13.15	3.63
2005	4	20.73	14.38	21.87	14.16	1377	0.9691	1.32	12.61	13.93	3.73
2005	5	23.71	14.86	24.80	14.19	1438	0.9675	1.18	14.13	15.31	3.91
2005	6	26.98	14.61	28.61	14.38	1437	0.9759	2.66	10.17	12.83	3.58
2005	7	29.22	14.38	31.06	14.22	1493	0.9787	3.36	8.73	12.09	3.48
2005	8	29.45	14.72	30.76	14.36	1472	0.9775	1.70	9.62	11.32	3.36
2005	9	26.87	14.30	28.14	14.08	1315	0.9739	1.64	10.56	12.20	3.49
2005	10	23.61	14.05	24.95	13.83	1509	0.9738	1.78	10.24	12.02	3.47
2005	11	20.34	14.33	22.02	14.37	1298	0.9756	2.81	10.03	12.83	3.58
2005	12	18.42	14.99	19.73	14.88	1441	0.9831	1.71	7.53	9.24	3.04

from those in ATOVS data (e.g. 700 hPa) a linear interpolation to the intermediate values is performed at the edges of each layer.

In the next step match-ups, i.e. temporally and spatially neighbouring observations of CHAMP and ATOVS are compiled. As CHAMP data consist of instantaneous observations we used accordingly individual ATOVS data which is neither averaged nor gridded and stems from only one satellite (Scan-oriented pixel-based data of NOAA-15). To define the next neighbour in both spatial and temporal context, a sort of translation between space and time is necessary. Fig. 8 may give an idea of the magnitude of such a space-time conversion. In this case the constant would be estimated by about 10 km/h. However, here integrative variances i.e. all possible time or space distances below a certain range are considered instead of the impact of a fixed distance in time or space. Moreover, the constant is expected to differ with height which is not considered in Fig.8.

The question here is whether it is worthwhile to derive an exact value for each vertical level and possibly also for each climate zone. The intended match-up list is reasonable also if not the absolutely nearest neighbour is taken. It would slightly enhance the scatter within the intended comparison, but no systematic shift would occur. The approximate time-space conversion constant can be estimated from Taylor hypothesis. The Taylor hypothesis assumes a frozen field travelling in space so that the time-space con-

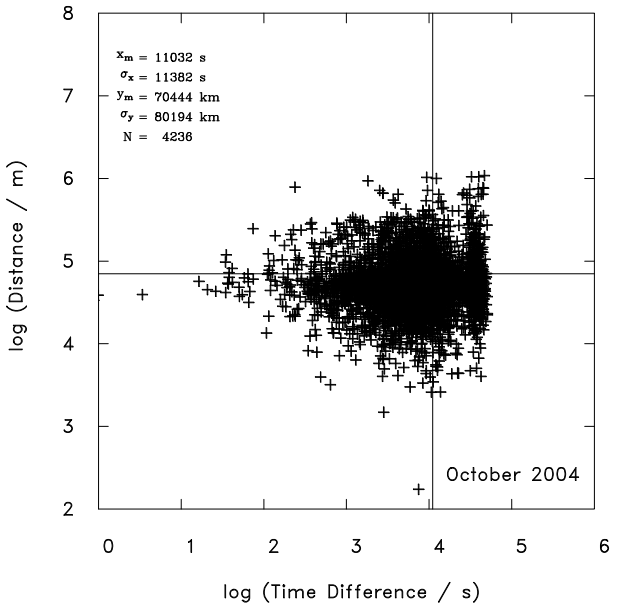

Figure 15: *Spatial and temporal distances of observation pairs from CHAMP and ATOVS in October 2004, given in logarithmic scales. Vertical and horizontal lines denote the average distances of about 3 hours and 70 km, respectively.*

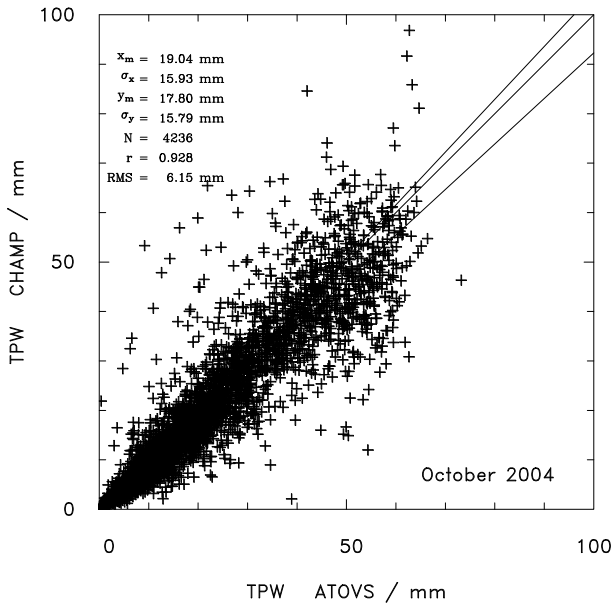

Figure 16: *Comparison of TPW from ATOVS with CHAMP observations. The data is based on match-ups using next neighbouring ATOVS observation from NOAA-15.*

version constant is equal to the travelling speed of the pattern. In the atmosphere this speed is about 10 ms^{-1}. In the following, we choose a slightly smaller value of 7.5 ms^{-1} for creating a match-up list of CHAMP and ATOVS observations.

Using a constant space-time conversion of 7.5 ms^{-1}, we determined for each CHAMP observation the nearest neighbour (in space and time) from ATOVS data. The mean occurring time difference is about 3 hours (11032 s), spatially the mean distance between the observation pairs is 70.4 km (Fig.15). The mean squared difference of observed water vapour includes an additive error measure for both satellites plus two contributions due to the temporal and spatial distances between the observations. The latter are expected to increase with growing temporal and spatial distance. Consequently, we fit the following

Table 4: Coefficients a, b, and c as obtained by fitting a linear function to the data for different vertical layers. a and b denote temporal and spatial factors of variance increase, c the variance for zero distance. For comparison, the actually observed moisture difference dm is given. The quotient a/b is an estimate for the conversion factor of temporal and spatial variance.

Layer	N	a mm^2s^{-1}	b mm^2m^{-1}	c mm^2	a/b m/s	dm mm^2
0	4239	1.215 10^{-3}	2.212 10^{-4}	8.80	5.49	37.79
5	3789	2.406 10^{-4}	4.852 10^{-5}	3.97	4.96	10.12
4	4074	1.356 10^{-4}	2.485 10^{-5}	2.16	5.45	5.43
3	4236	7.188 10^{-5}	1.273 10^{-5}	1.33	5.65	3.02
2	4236	1.381 10^{-5}	2.894 10^{-6}	0.26	4.77	0.61
1	4236	-2.982 10^{-7}	8.501 10^{-8}	0.01	-3.51	0.02

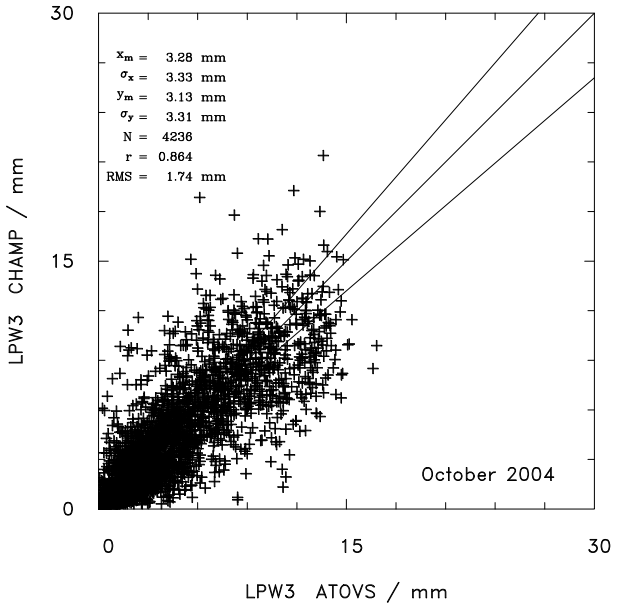

Figure 17: *As Fig.16, but for LPW 3 (700 - 500 hPa).*

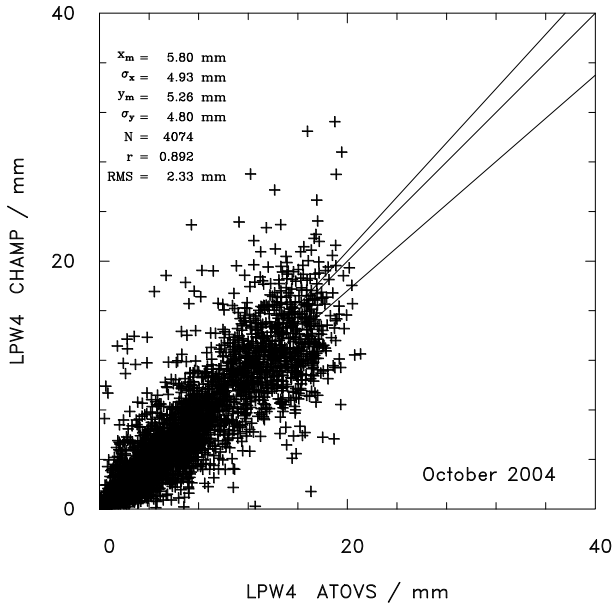

Figure 18: *As Fig.16, but for LPW 4 (850 - 700 hPa).*

linear function to the data:

$$\overline{\Delta LPW^2} = a\Delta t + b\Delta s + c \tag{9}$$

with Δt and Δs denoting temporal and spatial distances, respectively. In this way, three estimates are derived. The parameter c gives the error variance $\overline{\Delta LPW^2}$ for zero temporal and spatial distance, thus a minimum amount of rms, if exactly coinciding observations were available. Factors a and b describe the increase of error for growing temporal and spatial distances, respectively. Their quotient a/b is equal to the time-space conversion constant, preliminary set to 7.5 m/s. Results for the five layers plus TPW are summarized in Tab.4. The theoretical variance for zero distance (c) is roughly one third of the total squared difference actually obtained by the observations (dm). The other two thirds can be attributed to spatial and temporal distances between both observations. Both pure (c) and total errors (dm) decrease considerably with height. Consequently, also the temporal and spatial coefficients a and b become smaller, reflecting merely the decrease of variance with height. However, their quotient remains rather constant with about 5 ms^{-1}. In the highest layer an unphysically negative speed results from a negative time constant a. This means that differences in LPW do not grow with growing distances as usual. The large scatter of essencially time independent variance leads in this case to a even negative linear fit.

4.2 Difference statistics for match-ups

Figs. 16 to 18 show the scatter plots for match-ups of ATOVS and CHAMP observations. In October 2004 the available CHAMP observations differ systematically from their neighbouring ATOVS counterpart by 1.24 mm, corresponding to 7%. The wet bias is decreasing with height (Tab.5). In the mid atmosphere between 700 and 300 hPa (Layers 2 and 3) the relative error is nearly vanishing. In the top layer humidity is extremely low so that relative errors increase again and turn to dry biases of ATOVS. Results in Table 4 show that one third of the scatter arising in Figs. 16 to 18 is caused by observation

errors in both satellites.

Comparing the results from ATOVS-CHAMP match-ups (Tab.5) with those from the ATOVS-radiosondes comparison (Tab.2), a striking resemblance is obvious. ATOVS has a wet bias against both radiosonde and CHAMP observations, which increases for low atmospheric layers. Thus, concerning CHAMP data the conclusion of the match-up exercise can only be that their agreement to radiosondes is very high, although a direct comparison is not possible.

We extended the comparison of CHAMP/ATOVS data pairs to the complete year 2004. As it has turned out that the preliminary estimate of the conversion factor between temporal and spatial variability with 7.5 m/s was too large, we used in the following a reduced value of 5 m/s. As discussed above, the impact of such a change should be small. Marginal differences in our results after reducing the factor confirm this assumption. Of course, the mean temporal distances increase (from 11032 s to 12033 s) while spatial distance tend to become shorter (from 70 km to 65 km). However, the mean ATOVS TPW increases only from 19.04 to 19.05 m/s, the RMS is slightly increased from 6.15 to 6.18 mm, and the correlation remains nearly unchanged (compare Tab.5 and Tab.6 for October, both for Layer 0). From Tab.6 it is obvious that the features found in October 2004 are generally valid during the year. The TPW of CHAMP is smaller by 2 to 9 %. In the low atmosphere the difference is as high as 15%, decreasing with height. Above 500 hPa (layer 2) slight positive biases are found, escpecially in northern winter. Above 300 hPa (layer 1) the extreme low humidity is higher (by one half) if observed by CHAMP. However, an annual cycle of the differences is apparent. During northern summer the negative bias of CHAMP is at maximum, even if considered as relative value. This means for Layer 2, where the bias is generally reversed, that the differences to ATOVS are smallest in nothern summer. However, as ATOVS data is shown to be biased itself the possible conclusions remain limited.

4.3 Global maps of differences

ATOVS global humidity maps are produced by kriging which needs detailed information about errors and spatial correlation. In case of CHAMP data, such characteristics are difficult to derive, because temporally or spatially neighbouring observations do not exist internally. Consequently, global maps can only be produced if the temporal or spatial resolution is extreme low, which reduces on the other hand the representativeness of any individual observation. However, this study is more focussed on differences compared to ATOVS than on the absolute values. In this case, a much simpler and more direct approach can be used. Differences are expected to have a much smaller correlation length than the humidity itself. Even the assumption of completely uncorrelated differences would be reasonable. To produce fully covered maps is it therefore sufficient to apply for each observation an exponential reduction of influence, according to:

$$weight = e^{-\frac{d}{d_0}} \tag{10}$$

where d denotes the actual distance to the predicting point and d_0 a constant which determines the decrease of influence. This proceeding is equivalent to kriging, if errors are constant in space and redundancy of information from different observing points are neglected. For this special case the constant d_0 is equal to the correlation length. Often used by many authors, e.g. (Lindau, 2002), it is a convenient way to get an idea about the spatial distribution of a parameter.

Table 5: Mean water vapour in October 2004 as derived by match-ups of ATOVS and CHAMP. The bias is given absolute und relative magnitude. r and rms denote correlation coefficient and RMS difference, respectively.

Layer	ATOVS	CHAMP	bias mm	bias %	r	rms
0	19.04	17.80	1.25	7	0.928	6.15
5	10.29	9.00	1.29	14	0.928	3.18
4	5.80	5.26	0.53	10	0.892	2.33
3	3.28	3.13	0.14	5	0.864	1.74
2	0.83	0.85	-0.02	-2	0.738	0.78
1	0.07	0.09	-0.02	-27	0.463	0.13

Our aim is to produce global monthly maps of the moisture difference between CHAMP and ATOVS observation. The correlation length for daily TPW is about 600 km (Lindau, 2005), that for monthly means is expected to be higher. With 100 km, we choose d_0 much smaller than those values, because the difference measured by the two satellites is only weakly depended on their distance. On the other hand, d_0 should not be too small, in order to avoid a block diagram character of the map.

Figures 19 to 24 show the moisture difference between CHAMP and ATOVS in October 2004 for all layers, as obtained by the above described exponential data distribution. As already obvious from Fig.16 and Tab.6, the TPW shown in Fig.19 is characterised by a generally dryer atmosphere. However, Fig.19 shows additionally that the bias acts largely as a spatially constant factor. In the tropics where humidity is generally high, the difference to ATOVS is larger than in the cold Polar Regions. Extreme disagreements occur over Ethiopia and Indonesia. Such differences reflect in fact true problems of the satellites and are no technical artefact of our procedures. Over Ethiopia for example, 13 observations between 5°N and 10°N in latitude and 35°E and 45 °E in longitude are available. The mean difference of these pairs is as high as about 30 mm (22.3 mm for ATOVS and 51.2 mm for CHAMP). This difference is not caused by a single extreme value, because their standard deviations remain limited with 7.9 mm and 8.9 mm. The 13 observations pairs are temporally equally distributed over the month and differences in time and space are not suspect.

Referring back to Fig.3, where the monthly mean TPW of ATOVS is given, one may get some insight into this feature. Over East Africa a strong gradient in water vapour is striking. The reason is clearly the abrupt ascent from the Nile wetlands in Southern Sudan to the Ethiopian Highland with heights increasing from a few hundred to more that 4000 metres. The corresponding decrease of ATOVS TPW from 50.1 mm to 17.2 mm over only 270 km (over 3 grid cells from 34.04°E to 36.84°E) is absolutly plausible. Because CHAMP data have a lower spatial resolution the sharp moisture gradient is possibly not sufficiently resolved. This can explain the enormous humidity differences between CHAMP and ATOVS data (Fig.19), at least over Ethiopia.

With increasing height the bias diminishes. Layer 3 (700 to 500 hPa) is characterised by homogenously distributed scatter. However, here and even better visible in Layer 2, the amplitudes of scatter increase in low latitudes, where not only the moisture itself can be high, but also its variabilty is at maximum due to tropical convection cells. In the highest layer between 300 and 200 hPa (Fig.24) the moisture itself and the biases are extremely small. Both ATOVS and CHAMP measure values of less than 0.1 mm. As for the bottom layers, the difference acts as a global feature and can be described as a constant factor so that highest absolute values occur in the tropics.

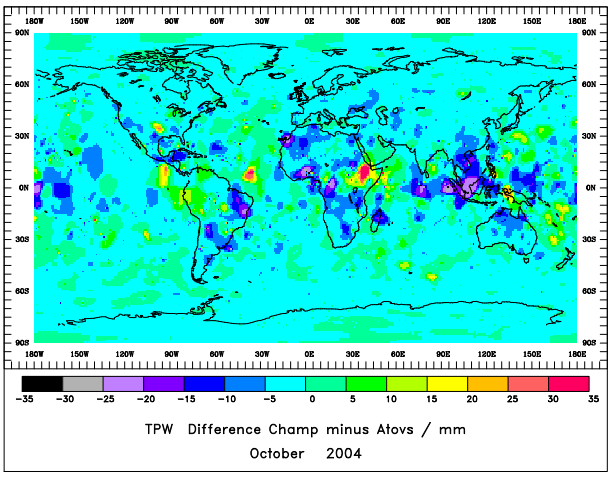

Figure 19: *Difference of Total Precipitable Water between CHAMP and ATOVS in October 2004.*

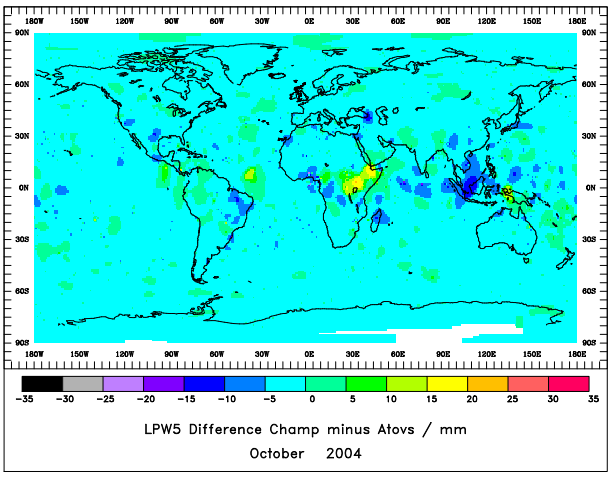

Figure 20: *As Fig.19, but for Layer 5 (1000 hPa - 850 hPa).*

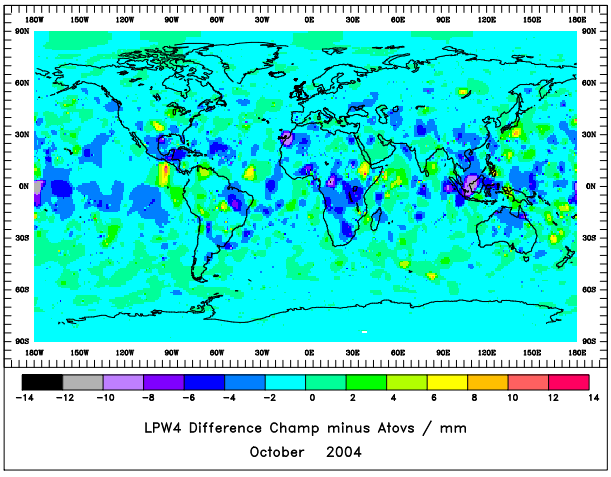

Figure 21: *As Fig.19, but for Layer 4 (850 hPa - 700 hPa).*

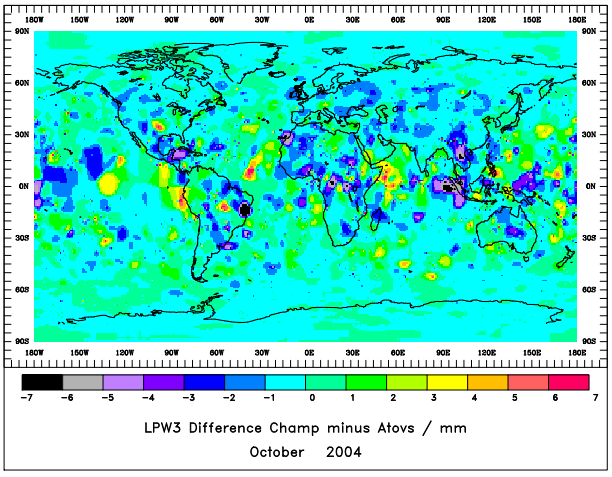

Figure 22: *As Fig.19, but for Layer 3 (700 hPa - 500 hPa).*

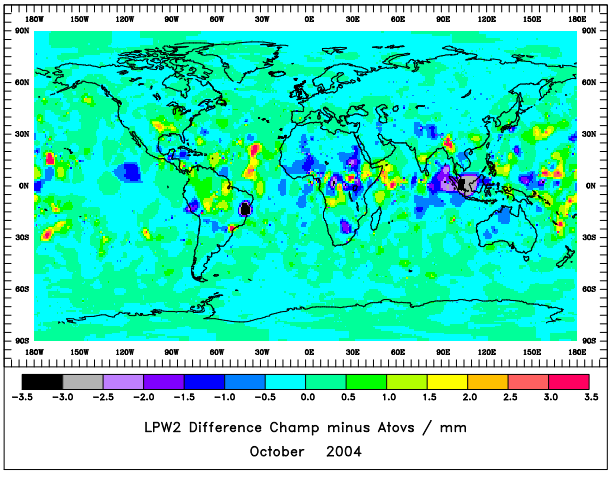

Figure 23: *As Fig.19, but for Layer 2 (500 hPa - 300 hPa).*

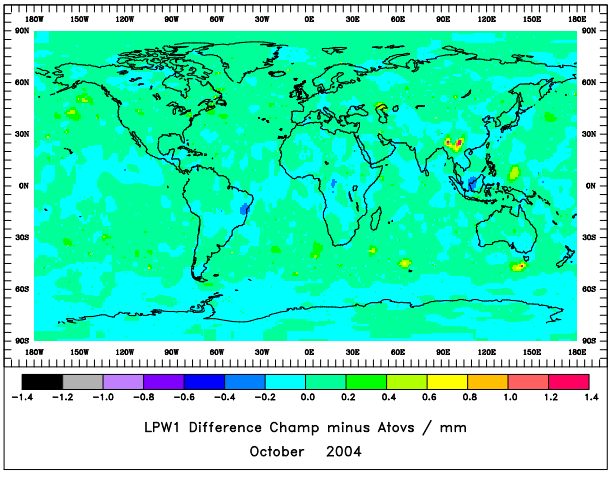

Figure 24: *As Fig.19, but for Layer 1 (300 hPa - 200 hPa).*

5 Conclusions

Three data sets of atmospheric humidity were investigated: Two satellite products from ATOVS and CHAMP and as ground truth radiosonde measurements were utilized. ATOVS data is shown to have a wet bias compared to radiosondes, strongest in the layer between 700 and 850 hPa, vanishing and even reversing with height. The overall bias for the entire atmosphere varies between 4% and 9% depending on the month considered. In the second lowest layer the wet bias amounts to about 10%, between 500 and 300 hPa the bias vanishes or is even slightly negative. In the uppermost layer over 300 hPa the bias is strongly negative throughout all considered months, although the absolute differences remain small in such dry regions of the atmosphere.

Compared to other satellite data, CHAMP is characterised by sparse data coverage providing only sporadic point measurements irregularly distributed over the globe. Therefore, a comparison to radiosondes was not directly possible. However, ATOVS data is nearly area covering and pairs of neighbouring observations from both satellites are compiled. Similar biases appear for these match-ups as they were found for the comparison between ATOVS and radiosondes. In the low layers CHAMP is dryer by about 10%; and similarly the bias is reduced from the bottom layer to vanishing or slightly positive differences in the higher atmosphere. Also the underestimation of ATOVS compared to radiosondes appearing again in the top layer is confirmed by CHAMP data.

Global maps of the monthly mean difference between ATOVS and CHAMP does not indicate any regions of specific problems. The found bias is rather homogeneously distributed over the globe and acts largely as a constant factor. However, in some regions strange large differences occur. Over Ethiopia they might be explained by the low spatial resolution of CHAMP data, but also other regions show area-limited, but strong disagreements, which need further employing GRAS data and newer versions of the ATOVS product.

References

Li, J., W. W. Wolf, W. P. Menzel, W. Zhang, H.-L. Huang, and T. H. Achtor, 2000: Global soundings of the atmosphere from ATOVS measurements: The algorithm and validation. J. Appl. Meteor., 39, 1248-1268.

Lindau, R. and E. Ruprecht, 2000: SSM/I-derived total vapour content over the Baltic Sea compared to independent data, Met.Zeitschrift, 9, No.2, 117-123.

Lindau, R., 2002: Energy and water balance of the Baltic Sea derived by merchant ship observations, Boreal Environment Research, 7 No.4, 417-424.

Lindau, R., 2003: Errors of Atlantic Air-Sea Fluxes Derived from Ship Observations, Journal of Climate, 16 No.4, 783-788.

Lindau, R. and J. Schulz, 2004: Gridding/merging techniques for the humidity composite product of the CM-SAF. Proceedings of the 2004 EUMETSAT Meteorological Satellite Conference, Prague, Czech Republic, EUM P41, 519-526.

Lindau, R., 2005: Optimal Merging of water vapour retrievals from different instruments (OMDI), Visiting Scientist Report, DWD, 33pp.

Wickert, J., T. Schmidt, G.Beyerle, R.Knig, C.Reigber and N. Jakowski, 2004: The Radio Occultation Experiment aboard CHAMP: Operational Data Analysis and Validation of Vertical Atmospheric Profiles. J. Meteorol. Soc. Jpn., 82, 381-395.

Table 6a: Statistical properties for the match-up comparison of CHAMP and ATOVS humidity. Statistical properties are given for each month of 2004 and each of the two highest vertical layers (1 - 2) plus the total atmospheric humidity (Layer 0). For the remaining layers see Tab.6b. Monthly mean (mean) and standard deviation (std) are given for ATOVS (A) and CHAMP (C) observations. N and r denote the number of pairs and the correlation coefficient, respectively. The bias (C-A) is given in mm and in relative measure ((C-A)/A).

Layer	Month	A mean	A std	C mean	C std	N	r	bias	rel bias
0	1	17.10	15.39	16.52	15.53	4121	0.899	-0.584	-3
0	2	16.73	15.61	16.47	15.68	3706	0.884	-0.260	-2
0	3	16.41	15.61	16.03	15.69	3948	0.858	-0.383	-2
0	4	16.72	15.47	16.34	15.79	4042	0.878	-0.379	-2
0	5	18.17	15.27	16.98	15.24	4237	0.929	-1.190	-7
0	6	19.39	15.05	17.64	14.45	3661	0.929	-1.747	-9
0	7	21.07	15.31	19.11	14.60	4022	0.916	-1.966	-9
0	8	21.67	15.86	19.67	15.09	3521	0.926	-2.000	-9
0	9	21.23	15.75	19.53	15.34	3917	0.923	-1.702	-8
0	10	19.05	15.93	17.80	15.79	4236	0.927	-1.256	-7
0	11	16.99	15.38	15.94	15.18	4209	0.922	-1.045	-6
0	12	16.17	15.03	15.35	15.19	4376	0.923	-0.820	-5
1	1	0.06	0.08	0.09	0.17	4121	0.426	0.031	48
1	2	0.06	0.08	0.09	0.22	3706	0.306	0.034	56
1	3	0.06	0.08	0.10	0.22	3948	0.308	0.040	64
1	4	0.06	0.07	0.09	0.18	4042	0.359	0.034	57
1	5	0.07	0.08	0.10	0.23	4237	0.353	0.035	53
1	6	0.07	0.08	0.10	0.17	3661	0.432	0.032	49
1	7	0.07	0.08	0.12	0.25	4022	0.264	0.046	63
1	8	0.08	0.09	0.13	0.22	3521	0.398	0.046	59
1	9	0.07	0.08	0.10	0.17	3917	0.416	0.030	41
1	10	0.07	0.08	0.09	0.14	4236	0.458	0.025	38
1	11	0.06	0.07	0.08	0.13	4209	0.491	0.021	35
1	12	0.06	0.08	0.08	0.17	4376	0.430	0.023	38
2	1	0.79	0.97	0.87	1.26	4121	0.671	0.075	9
2	2	0.74	0.95	0.82	1.30	3706	0.625	0.079	11
2	3	0.77	0.98	0.82	1.18	3948	0.667	0.051	7
2	4	0.77	0.93	0.84	1.18	4042	0.669	0.071	9
2	5	0.84	0.99	0.86	1.19	4237	0.765	0.018	2
2	6	0.86	0.99	0.85	1.20	3661	0.707	-0.010	-1
2	7	0.96	1.08	0.97	1.43	4022	0.645	0.008	1
2	8	1.00	1.19	1.03	1.44	3521	0.726	0.024	2
2	9	0.94	1.06	0.96	1.31	3917	0.720	0.025	3
2	10	0.83	0.96	0.85	1.14	4236	0.732	0.017	2
2	11	0.76	0.94	0.79	1.08	4209	0.747	0.028	4
2	12	0.74	0.94	0.77	1.18	4376	0.706	0.028	4

Table 6b: As Tab.6a, but for the lower atmospheric layers (3 - 5).

Layer	Month	A mean	A std	C mean	C std	N	r	bias	rel bias
3	1	2.94	3.20	2.93	3.28	4121	0.807	-0.012	0
3	2	2.77	3.12	2.81	3.22	3706	0.788	0.035	1
3	3	2.86	3.29	2.84	3.28	3948	0.771	-0.026	-1
3	4	2.97	3.13	2.93	3.19	4041	0.810	-0.038	-1
3	5	3.17	3.17	3.03	3.21	4237	0.847	-0.135	-4
3	6	3.32	3.20	3.08	3.08	3661	0.846	-0.233	-7
3	7	3.71	3.40	3.42	3.26	4022	0.856	-0.287	-8
3	8	3.80	3.62	3.58	3.46	3521	0.853	-0.216	-6
3	9	3.67	3.48	3.49	3.33	3917	0.859	-0.181	-5
3	10	3.28	3.32	3.13	3.31	4236	0.861	-0.144	-4
3	11	2.89	3.21	2.79	3.15	4209	0.849	-0.102	-4
3	12	2.78	3.10	2.68	3.16	4376	0.826	-0.098	-4
4	1	5.24	4.77	4.88	4.76	3948	0.867	-0.358	-7
4	2	5.01	4.73	4.74	4.72	3577	0.838	-0.265	-5
4	3	4.97	4.83	4.71	4.79	3797	0.812	-0.254	-5
4	4	5.20	4.75	4.92	4.84	3879	0.834	-0.278	-5
4	5	5.54	4.65	5.06	4.66	4047	0.870	-0.478	-9
4	6	6.01	4.59	5.32	4.34	3492	0.873	-0.685	-11
4	7	6.64	4.74	5.84	4.40	3824	0.871	-0.800	-12
4	8	6.80	4.99	5.94	4.59	3376	0.879	-0.858	-13
4	9	6.52	4.88	5.79	4.65	3785	0.883	-0.736	-11
4	10	5.79	4.92	5.26	4.80	4076	0.890	-0.531	-9
4	11	5.17	4.76	4.66	4.58	4032	0.884	-0.504	-10
4	12	4.95	4.66	4.48	4.62	4203	0.879	-0.471	-10
5	1	9.35	7.64	8.44	7.42	3605	0.901	-0.901	-10
5	2	9.28	7.91	8.56	7.59	3297	0.882	-0.727	-8
5	3	8.79	7.79	8.12	7.48	3519	0.864	-0.673	-8
5	4	8.96	7.79	8.29	7.57	3528	0.871	-0.668	-7
5	5	9.83	7.44	8.60	7.20	3754	0.925	-1.228	-12
5	6	10.61	7.27	9.03	6.77	3232	0.925	-1.578	-15
5	7	11.37	7.15	9.70	6.66	3516	0.902	-1.670	-15
5	8	11.51	7.36	9.73	6.81	3120	0.914	-1.785	-16
5	9	11.17	7.62	9.66	7.19	3556	0.914	-1.507	-13
5	10	10.29	7.79	9.00	7.37	3791	0.928	-1.290	-13
5	11	9.30	7.56	8.22	7.19	3735	0.921	-1.088	-12
5	12	8.77	7.43	7.95	7.27	3881	0.919	-0.826	-9